Immersion cooling fluid comparison using a single-phase immersion/liquid technique for data centers

Ayoub Ruichek, Mohamad Hnayno, Ali Chehade, Farouk Fardoun, Tala Moussa, Guillaume Polidori, Chadi Maalouf

Applied Thermal Engineering 280 (2025) 128355

Contents lists available at ScienceDirect

Applied Thermal Engineering

journal homepage: www.elsevier.com/locate/apthermeng

Research Paper

Immersion cooling fluid comparison using a single-phase immersion/liquid technique for data centers

Ayoub Ruichek [a,c,*], Mohamad Hnayno [a,*], Ali Chehade [a], Farouk Fardoun [b], Tala Moussa [c], Guillaume Polidori [c], Chadi Maalouf [c]

[a] OVHcloud, 155 Avenue Georges Hannart, 59170 Croix, France
[b] Doctoral School of Science and Technology Lebanese University, Hadath, Lebanon
[c] ITHEMM, University of Reims Champagne-Ardenne, 51100 Reims, France

ARTICLE INFO

Keywords:
Datacenter cooling
Single-phase immersion cooling
Natural convection
Dielectric fluid
Thermophysical property
Figure of Merit
Heat transfer

ABSTRACT

This paper analyses the cooling performance of different immersion fluids for a single-phase immersion/liquid-cooling technique, which integrates a direct-to-chip water-cooling system with passive single-immersion cooling technology. The choice of dielectric fluid is a key factor in determining heat dissipation performance, as its thermophysical properties directly affect cooling efficiency. An experimental setup tested the impact of four dielectric fluids — SL 3568 (Shell), FES 822–6542 (Fuchs), EGEN 100R8 (Motul) and BioLife 4 (TotalEnergies Fluids) — on the thermal behavior of the system. The selection of these dielectric fluids offers insights into different development focuses such as diverse viscosity grades, flash point and biodegradability. The impact of the Figure of Merit for Natural Convection (FOM1), developed by the Open Compute Project (OCP) Immersion Cooling Sub-Project to assess the combined influence of fluid properties, was discussed and used as an evaluation indicator to investigate the impact of the dielectric fluids on the IT equipment. The results indicate that approximately doubling the FOM1 value (when comparing BioLife 4 to SL 3568) reduces the Prandtl number by around a factor of ten. This enhancement translates into notable thermal improvements for components directly immersed in the dielectric fluids, with RAMs, NVMEs, and SSDs exhibiting temperature reductions of approximately 6.7 °C, 6.4 °C, and 5.9 °C, respectively. Conversely, CPU temperatures were found to be highest when using fluids with elevated FOM1 values. Since the CPUs are cooled via cold plates and not in direct contact with the immersion fluid, this trend is attributed to the possible infiltration of the dielectric fluid into the thermal interface material applied between the CPUs and the cold plates. Such infiltration appears to significantly reduce the viscosity of the TIM, by at least 94.4 %, thereby degrading its thermal performance. To enable a more extensive evaluation of immersion fluids available in the industry, a numerical simulation of the fluid flow and thermal behavior of the IT equipment within the hybrid system was conducted and validated against experimental results.

1. Introduction

With the rapid expansion of cloud computing and AI technology, the number of high-performance operational data centers (DCs) has increased rapidly, reaching 700 facilities in 2021 [1]. As a result, the electrical energy demand of DCs has increased sharply. According to International Energy Agency (IEA), DCs consumed about 460 TWh in 2022, accounting for nearly 2 % of global electricity consumption [2]. This figure is projected to rise to 752 TWh by 2030 [3,4]. A substantial portion of this energy, up to 40 %, is attributed to cooling systems, which are essential for maintaining optimal operating temperatures and preventing equipment failure due to overheating [5]. However, these systems are also among the most energy-intensive devices of DC infrastructure, primarily due to the high power requirements of conventional cooling technologies [6]. In response to these challenges, significant research is underway to develop more energy-efficient and innovative cooling techniques.

Air cooling, the most widely adopted method, relies on fans to direct airflow over electronic components to dissipate heat [7,8]. However, the heat transfer limitations of traditional air cooling are inadequate for

* Corresponding authors.
E-mail addresses: ayoub.ruichek@ovhcloud.com (A. Ruichek), mohamad.hnayno@ovhcloud.com (M. Hnayno).

https://doi.org/10.1016/j.applthermaleng.2025.128355
Received 9 July 2025; Received in revised form 2 September 2025; Accepted 13 September 2025
Available online 17 September 2025

meeting the requirements of low-power, high-efficient, and eco-friendly DCs. Specifically, the cooling capacity of air-based cooling systems is typically restricted to below 37 W/cm^2, posing a significant limitation especially for high-performance computing [9,10].

Liquid cooling systems have appeared as a more efficient alternative, offering enhanced heat absorption and dissipation capabilities [11]. With cooling capacities exceeding 100 W/cm^2 [12], these systems utilize fluids with higher densities and thermal conductivities than air [13]. Liquid cooling can be categorized into indirect and direct liquid cooling approaches [14]. In indirect liquid cooling, the coolant circulates through cold plates affixed to the main heat-generating IT components, such as central processing units (CPUs) and graphical processing units (GPUs) [15,16]. However, with new and more powerful server profiles, more disks and RAMs are being integrated. In this context, implementing cold plate would require additional space and often necessitate multiple custom designs to accommodate the diverse hardware configurations [17].

On the other hand, direct liquid cooling —specifically immersion cooling— submerges IT components in a thermally and non-electrically conductive fluid, allowing for direct contact with all surfaces. This approach substantially increases the effective heat transfer area and significantly enhances cooling performance [18]. According to existing literature, immersion cooling can be classified into single-phase immersion cooling (SPIC) and two-phase immersion cooling (TPIC), depending on the thermal behavior of the dielectric coolant when exposed to heat generated by electronic components [19,20]. In SPIC systems, servers are entirely submerged in the dielectric fluid that will cool them by convection, without undergoing a phase change. To ensure that the coolant remains in the liquid phase throughout operation, high-boiling-point fluids are typically employed [21]. SPIC configurations are further divided into two categories: gravity-driven systems [22], which rely on natural convection, and pump-driven systems, where the immersion coolant is actively circulated by pumps [23]. While pump-driven systems generally offer higher heat dissipation efficiency compared to natural convection systems, careful optimization of the pump and its control is essential to minimize power consumption, as demonstrated by Sun et al. [24] and Liu et al. [25]. Conversely, TPIC systems utilize low-boiling-point dielectric fluids that undergo phase transition during operation. Upon direct contact with heated server components, the fluid begins to boil, forming vapor that rises to a condenser located at the top of the tank. The vapor subsequently condenses and returns to the liquid phase, enabling continuous cooling [26].

While TPIC offers enhanced heat transfer through latent heat absorption, it often requires more complex design and operation, presenting maintenance difficulties and high costs. From an economic and practical standpoint, SPIC is more favorably positioned for large-scale deployment than TPIC [26]. Consequently, current research in immersion cooling predominantly focus on the development and optimization of SPIC systems.

Recent literature identifies several categories of immersion coolants commonly used in SPIC systems, including fluorinated electronic liquids, oil-based coolants, and nanofluids [27]. Numerous comparative studies have been conducted to evaluate the thermal performance of these fluids, with a focus on their thermal properties. Pambudi et al. [28] experimentally investigated the cooling effectiveness of mineral oil (MO) and virgin coconut oil (VCO) as coolants for a SPIC system. The results indicated that the MO achieved a lower temperature of 47 °C at maximum CPU temperature, compared to 51 °C for VCO. Luo et al. [29] conducted a computational analysis comparing the thermal performance of silicon carbide (SiC) oil-based nanofluids with conventional mineral oil in SPIC systems. The study demonstrated a significant enhancement in thermal conductivity with the use of SiC nanofluids. However, it was also noted that increasing nanoparticle concentration led to a reduction in specific heat capacity, thereby diminishing overall heat transfer efficiency, particularly at low flow rates. Dharanegowda et al. [21] performed an experimental evaluation of deionized water, mineral oil, and propylene glycol in SPIC systems, assessing their thermal performance across varying flow rates and heat inputs. The findings showed that deionized water outperformed the other fluids, maintaining the lowest outlet temperature under all test conditions, attributed to its superior thermal conductivity and specific heat capacity.

Shrigondekar et al. [30] carried out both experimental and numerical investigations to compare the thermal performance of FC-40 dielectric fluid and PAO-6 dielectric oil in SPIC systems for a 1U server. The study examined the influence of parameters such as fluid flow rate, inlet temperature, and heat load. The results indicated that PAO-6 exhibited superior heat transfer performance at higher flow rates, whereas FC-40 was more effective under lower flow conditions. The higher viscosity of PAO-6 was identified as a key factor influencing its thermal behavior. Chen et al. [31] performed a numerical analysis of electronic fluorinated liquids (EFLs) in SPIC systems, comparing three different fluids—EFL-F1, EFL-F2, and EFL-F3—to assess their heat transfer characteristics and flow behavior. The findings demonstrated that fluids with lower dynamic viscosity, such as EFL-F1, enhanced heat transfer efficiency and minimized pressure losses, thereby improving overall system performance. Conversely, despite its high thermal conductivity, EFL-F3′s elevated viscosity resulted in reduced cooling efficiency. Kim et al. [32] conducted a computational investigation into the thermal performance of nine different dielectric fluids in single-phase immersion cooling (SPIC) systems. Among the fluids evaluated, TMC-7200 —characterized by the lowest dynamic viscosity— was found to be the most effective in reducing CPU temperatures. Alkasmoul et al. [33] performed a numerical study comparing the thermal behavior of Al_2O_3–water, TiO_2–water, and CuO–water nanofluids in SPIC systems designed for data center servers. The findings demonstrated that the Al_2O_3–water nanofluid provided the best thermal performance due to its high thermal conductivity, resulting in a significant reduction in CPU temperatures. However, the study also highlighted that its elevated viscosity contributed to higher pressure drops and increased pumping power requirements.

Validating immersion fluids for cooling IT equipment remains a key strategy within the industry. Given the wide variety of dielectric liquids currently in use, a systematic evaluation is necessary to ensure these fluids meet the thermal performance requirements of modern DC environments. For this reason, the Immersion Cooling Sub-Project from the Open Compute Project (OCP) is actively developing specifications outlining the thermal performance requirements for immersion coolants used in IT equipment cooling [34]. This standardization effort aims to enable the IT industry to evaluate and identify the most suitable immersion fluids by balancing performance with economic considerations. Dimensionless Figures of Merit (FOMs) are defined in the OCP Base Specification for immersion fluids, for Natural Convection (FOM1) and Forced Convection (FOM2). These indicators represent respectively the natural convection and the forced convection effectiveness for immersion liquids. FOMs can be used to evaluate and compare the thermal performance of several candidate immersion cooling fluids and hence guide the selection and optimization of dielectric fluids. FOM1 is used as an evaluation indicator in this study. This metric is derived from Nusselt number correlation for heatsink with vertically oriented plate-fins [35]. It can be defined as:

$$FOM1 = k\left(\frac{\beta c_p \rho 2}{\mu k}\right)^{0.2813} \quad (1)$$

where k is the thermal conductivity (W.m^{-1}.K^{-1}), β is the thermal expansion coefficient (K^{-1}), c_p is the specific heat (J.kg^{-1}.K^{-1}), ρ is the density (kg.m^{-3}) and μ is dynamic viscosity (Pa.s) of the immersion fluids.

This study advances the evaluation of immersion cooling fluids by considering the combined influence of multiple fluid properties, rather than a single parameter. The use of FOM1 as an evaluation indicator

provides a more comprehensive assessment, allowing the identification of fluids with enhanced overall heat dissipation capabilities. This paper aims to compare experimentally the cooling performances of four fluids for immersion cooling by using these metrics to analyze the thermal behavior of a 620 W server submerged in a single-phase immersion/liquid cooling system. Furthermore, this criterion is compared with other more conventional indicators, such as the Rayleigh number and the Prandtl number, to assess whether it reliably reflects the effectiveness of natural convection for an immersion fluid. In addition, a numerical investigation was conducted to assess the thermal behavior of the fluid and IT equipment in the hybrid system with a chosen immersion fluid (SL 3568). The CFD model was validated against experimental data to enable a more extensive evaluation of a range of immersion coolants available in the industry.

2. System description

Each server is submerged in its own tank for independent cooling, as shown in Fig. 1 a). The server rack design contains up to 48 servers (1U) or 24 servers (2U), with 3 stacks. The immersion cooling (IC) rack is shown in Fig. 1 b). A pumping substation (PSS) ensures the pumping of water to the racks and a dry cooler are used to cool the water supplied to the PSS and evacuate heat outside the DC. While CPUs, which are the most power-consuming components in servers, are cooled by using cold plates (also called water blocks (WBs)), other IT components in the server (such as RAMs and disks) are cooled by the dielectric fluid via natural convection. Additionally, a serpentine convection coil communicates with the WBs through a closed-loop circuit and forms a significant exchange surface for cooling the dielectric coolant. One possible circuit configuration is to circulate the water from WBs to serpentine.

This novel technology supports high-power racks with cooling capacities of up to 54 kW and accommodates inlet temperatures as high as 45 °C, thereby removing the need for evaporative cooling systems at the dry coolers level and ensuring reliable operation across a wide range of climatic conditions. Moreover, a 20 K water temperature differential can be achieved due to its high thermal efficiency. The system achieves a cooling partial Power Usage Effectiveness (pPUE) of 1.004 and reduces water consumption (WUE) to zero. Furthermore, the technology enhances heat recovery, that leads to new opportunities for energy valorization. The passive rack design without fans contributes to a quieter DC environment and lower operational expenditure (OPEX). Additionally, the hybrid system achieves a compact footprint of up to 37 U/m^2, supporting higher compute density. By employing dielectric fluids with low ozone depletion potential (ODP) and global warming potential (GWP), this solution aligns with increasing demands for environmental sustainability [36].

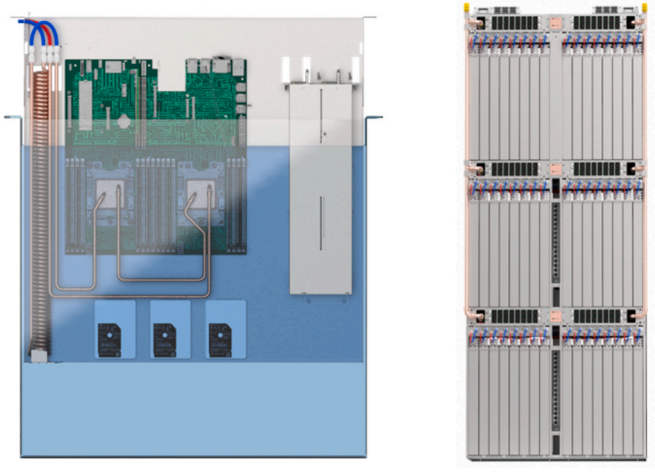

Fig. 1. A) hybrid immersion liquid cooling system, b) immersion cooling rack (48 servers).

In the following section, an experimental setup was used to examine the effects of 4 dielectric fluids —SL 3568, FES 822–6542, EGEN 100R8, and BioLife 4— within the hybrid system. The Figure of Merit for Natural Convection FOM1, developed by the OCP Immersion Cooling Sub-Project to evaluate the combined influence of thermophysical properties, was validated and adopted as an assessment metric to investigate the impact of the dielectric fluids on IT equipment performance.

3. Fluids comparison experimental test

3.1. Experimental setup and procedure

An Intel-based 1U open computing server with a total power consumption of 620 W is used. The server was configured with two CPUs, twelve RAM modules, and six NVME disks. Four dielectric fluids which differ in their development focus were investigated: SL 3568, FES 822–6542, EGEN 100R8 and BioLife 4. Their chemical and physical properties are listed in Table 1.

The water-cooling system consists of a primary cooling circuit and a secondary cooling circuit, as represented in Fig. 2 a). In the primary cooling circuit, water coolant is pumped to cool the immersed server using a Cooling Distribution Unit (CDU) consists of a pump and a Plate Heat Exchanger (PHEX). In this regard, a serpentine convection coil, with a diameter of 30 mm and linear length of 5.8 m, is connected to the WBs through the primary circuit and cools the immersion coolant by natural convection. Water flows from the WBs to the serpentine coil. The heated water then passes through the PHEX to transfer heat to the secondary cooling water circuit. The latter is connected to a dry cooler to evacuate heat outside the DC.

The server is immersed in dielectric fluid, which is contained in an insulated tank of 600 × 500 × 50 mm^3 to avoid heat transfer between the tank and the environment. It should be noted that the heat transfer between fluids and the server can be considered as natural convection since no pump was used to circulate the dielectric coolant around the IT equipment.

The experimental setup, including the sensor distribution illustrated in Fig. 2 a) and b) was implemented in an IC lab within the OVHcloud experimental DC in Croix-France. This setup was designed to investigate the impact of different dielectric fluids on an operational server. The tests were accompanied by temperature, flow rate, pressure and differential pressure measurements. All sensors were connected to a compact DAQ data acquisition system.

A thermocouple is used to measure the ambient temperature of the IC

Table 1
Thermophysical properties of the dielectric fluids used in the experiments.

Properties	SL 3568	FES 822–6542	EGEN 100R8	BioLife 4
Company	Shell	Fuchs	Motul	TotalEnergies Fluids
Colour & Odour	Colourless / Odourless			
Kinematic viscosity* (mm^2.s^{-1})	43	11.5	8.1	4
Flash point (°C)	265	204	166	145
Density* (kg.m^{-3})	811	813	787	771
Specific heat* (kJ.kg^{-1} K^{-1})	2.00	2.25	2.24	2.235
Thermal conductivity* (W.m^{-1}.K^{-1})	0.139	0.134	0.140	0.138
Thermal diffusivity* (0.10^{-8} m^2.s^{-1})	8.6	7.3	7.9	8
Expansion rate* (K^{-1})	0.00065	0.0008	0.0009	0.00071
Environmental Ecology	Ultra-low vaporization / Nontoxic and Non allergenic			
Biodegradability (28 Days)			> 60 %	88 %

*Properties are taken at a reference temperature of 40 °C, as it is the expected average fluid temperature in an immersion cooling system.

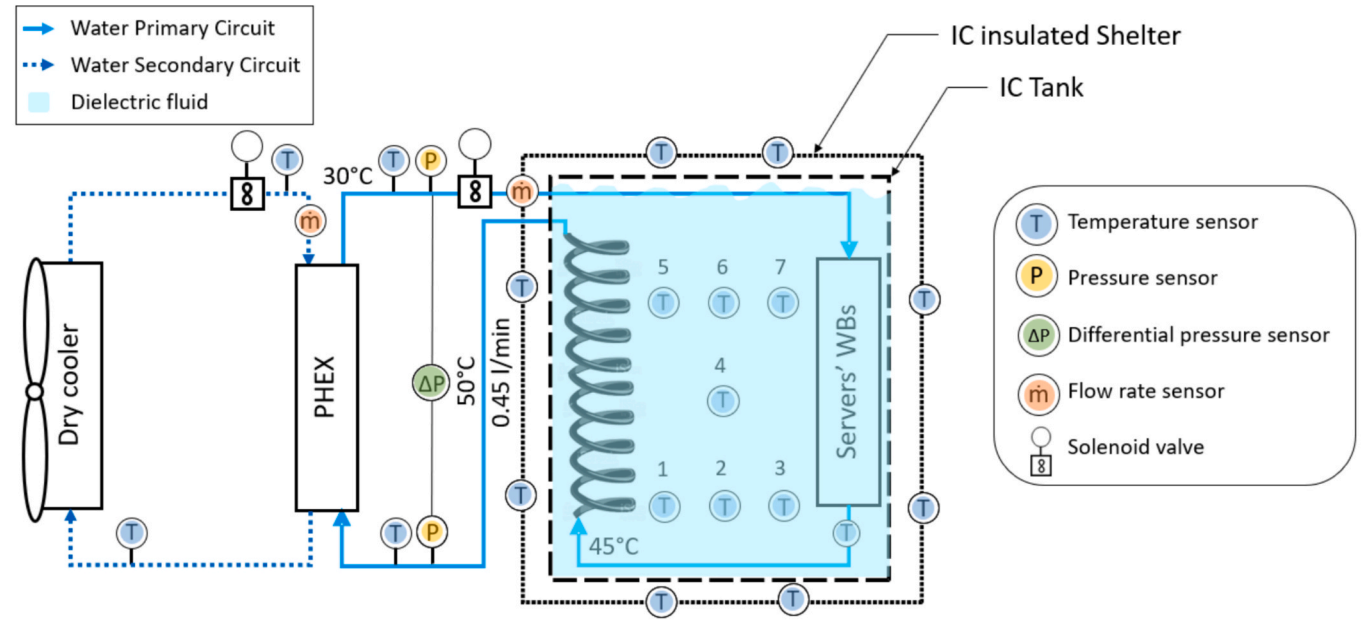

a)

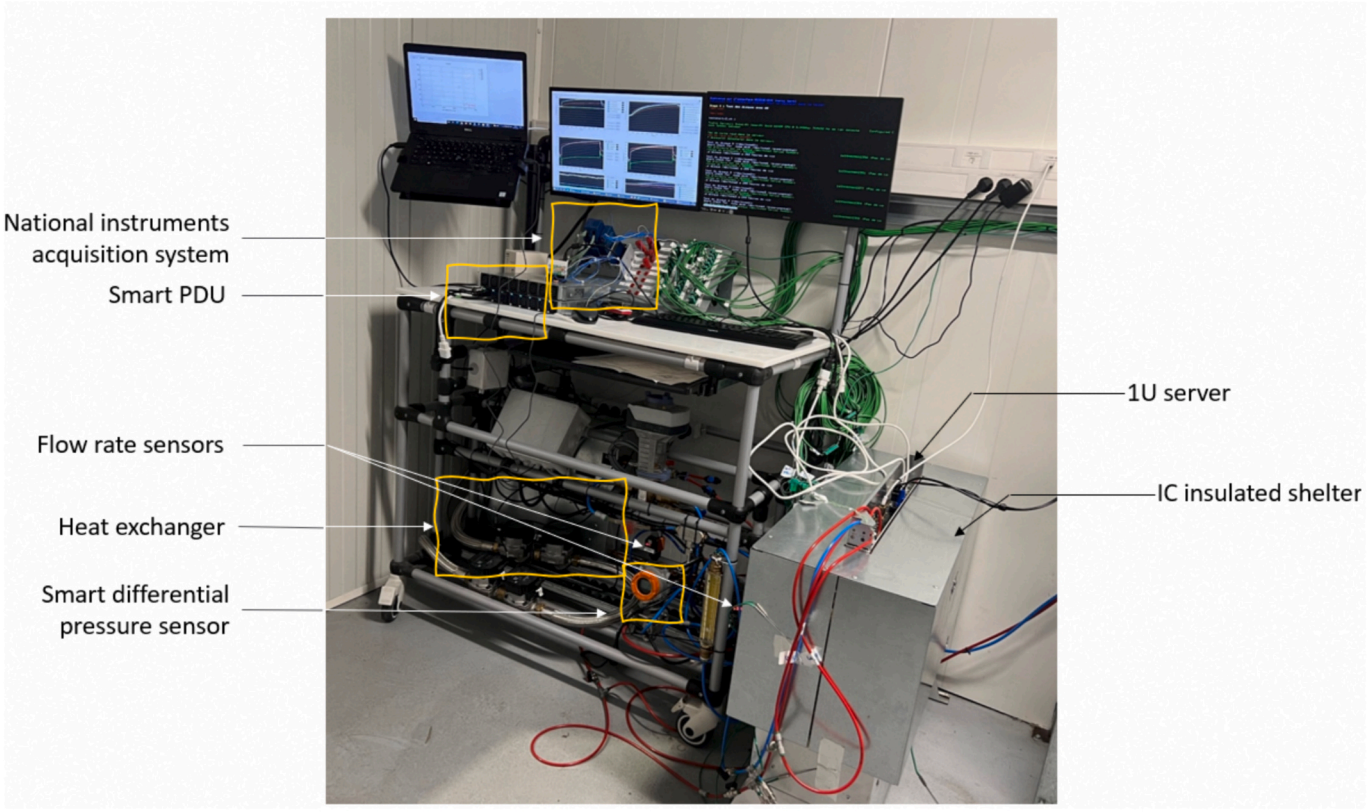

b)

Fig. 2. A) experimental setup scheme of the ic lab, b) photo of the experimental setup.

lab. Besides, seven thermocouples were installed inside the tank to measure the fluid temperature. It should be noted that eight thermocouples were installed on the wall surfaces to measure the shelter wall temperatures. Therefore, the heat losses were estimated to be negligible. Additionally, thermocouples measured the inlet and outlet of the water-cooling circuit and the pipelines of each component (serpentine, WBs, and dry cooler). All the temperature sensors were type-K thermocouples with an accuracy of ± 0.210 °C after calibration. The temperature

measurement devices were calibrated by using a high-precision temperature sensor as reference.

Two Kobold flow-rate sensors (0.05–10 l.min^{-1}) were installed on secondary and primary circuits to measure the cold-water flow rate feeding the heat exchanger and the IC tank. Two Kobold pressure sensors (0–6 bar) were installed at the IC tank inlet and outlet. A Kobold differential pressure sensor (3.73–373 mbar) was installed on the IC tank circuit inlet and outlet to measure the pressure drops across the serpentine and WBs.

A high-accuracy solenoid valve was installed in the secondary circuit, integrated with a temperature probe, to ensure a smooth regulation of the supplied water temperature in the primary circuit.

The operating procedure of the experimental setup is summarized as follows:

1. Before experiments, the experimental loop circuits were fully filled with pure water. Air was then vented from the high points of the circuit, ensuring an entire air-free system.
2. The water flow rate supplied in the primary circuit was manually adjusted for each test.
3. The inlet temperature of cooling water was regulated by controlling the flow rate in the secondary circuit, which connected to the dry cooler.
4. A flexible I/O (fio) tester script was used to apply computational stress to the server components. An Intelligent Platform Management Interface (IPMI), a standardized interface for monitoring and managing hardware independently of the operating system, was employed to collect real-time data from the IT components (CPU and memory temperatures, IT individual power consumption, CPU frequency, RAM bandwidth, and other performance metrics).
5. The server power was measured continuously with a time step of 1 s using a power distribution unit (PDU).

Each evaluation test was experimentally characterized by varying the water flow rate and the inlet water temperature from 30 to 45 °C in 5 °C increments. Flow rates in both the primary and secondary circuits were recorded. The measurements were monitored using a data acquisition system at a frequency of 1 Hz (one sample per second). Fluid temperatures were reported when all the measurements reached steady-state conditions.

The thermal heat load was estimated as:

$$Q = \dot{m}\, Cp\, \Delta T \tag{2}$$

where $\dot{m}$ (kg.s^{-1}) is the water mass flow rate, Cp (kJ.kg^{-1}.°C^{-1}) is the specific heat of water, and ΔT (K) is the water temperature difference in the server water circuit.

Absolute pressure sensors, differential pressure sensors, thermocouples and flow rate sensors calibrations are carried out by comparing the response measured by each component to those measured by high precision sensor probes. Uncertainties are evaluated using the method of Kline and McClintock [37]. For example, the uncertainty of the thermal heat load (Q) is evaluated by:

$$\Delta Q = \sqrt{\left[\left(\frac{\partial Q}{\partial \dot{m}}\Delta \dot{m}\right)^2 + \left(\frac{\partial Q}{\partial T_1}\Delta T_1\right)^2 + \left(\frac{\partial Q}{\partial T_2}\Delta T_2\right)^2\right]} \tag{3}$$

where $\dot{m}$ is the water flow rate, T_1 is the inlet temperature, T_2 is the outlet temperature while $\Delta\dot{m}$, ΔT_1 and ΔT_2 denote their respective absolute uncertainties.

Uncertainties for measured parameters are given in Table 2.

Table 2
Uncertainties for measured parameters.

Parameter	Uncertainty
Temperature, $\boldsymbol{T}$ (°C)	±0.210 °C
Pressure, $\boldsymbol{P}$ (Pa)	±0.5 %
Differential pressure, $\Delta\boldsymbol{P}$ (Pa)	±0.25 %
Flow rate, $\dot{\boldsymbol{m}}$ (l.min^{-1})	±1 %
Heat load, $\boldsymbol{Q}$ (W)	±1.8 %

3.2. Results and discussion

3.2.1. FOM1 Criteria evaluation

FOM1s are calculated for the four selected immersion fluids at 40 °C and the corresponding values are plotted in Fig. 3. It is evident that SL 3568 exhibits the lowest cooling capability, whereas BioLife 4, with the lowest viscosity and flash point compared to the other fluids, demonstrates the highest cooling capability for buoyancy-driven immersion cooling system, as indicated by its maximum FOM1 value. This suggests that heat diffusion within this fluid would be more efficient relative to the other fluids.

Nevertheless, as noticed from Table 1, BioLife 4 does not possess the highest thermal diffusivity. In static conditions, fluids with higher thermal diffusivity diffuse heat more effectively. However, under dynamic conditions involving fluid motion, thermal diffusivity must be considered in conjunction with momentum diffusion, which is influenced by viscosity and can hinder the flow. Hence, Prandtl number is used to evaluate the relative effects of viscosity and thermal diffusion within the fluid.

Prandtl number can be expressed as:

$$Pr = \frac{\nu}{\alpha} \tag{4}$$

where ν is the kinematic viscosity (m^2.s^{-1}) and α is thermal diffusion (m^2.s^{-1}) of the fluid.

Fig. 4 shows the Prandtl numbers associated with the four immersion fluids. BioLife 4, which exhibits the highest FOM1, is also characterized by the lowest Prandtl number among the fluids studied. Moreover, the influence of viscosity on heat diffusion in SL 3568 is approximately three, five and ten times greater than in FES 822–6542, EGEN 100R8 and BioLife 4, respectively. This suggests that the viscosity of BioLife 4 has the least impact on heat diffusion. In contrast, fluids with higher Prandtl numbers, such as SL 3568, indicate that their temperature fields are more strongly influenced by viscosity forces than fluids with lower Prandtl numbers. Furthermore, the four considered fluids exhibit relatively high Prandtl numbers (ranging from 50 to 502), which indicates that in all cases the thermal boundary layer remains thinner than the velocity boundary layer. Nevertheless, a decrease in the Prandtl number increases the ratio of thermal to velocity boundary layer thicknesses, leading to a slight relative thickening of the thermal boundary layer [38]. While this effect locally reduces the near-wall convection around IT components, the reduction in Prandtl number is primarily driven by a decrease in viscosity, which strongly enhances buoyancy forces at the tank scale. This increase in flow intensity largely compensates for the local weakening of heat transfer near the wall, so that fluids with lower Prandtl numbers can promote more vigorous convective transport. This analysis underscores the importance of taking a global view of the thermo-fluidic properties to better assess the relative influences of viscosity and thermal diffusivity for each of the fluids studied.

Furthermore, Rayleigh number is the common dimensionless number used to characterize the flow and heat transfer regime of the immersion coolants in natural convection, under the effect of buoyancy forces and a temperature difference.

Rayleigh number is defined as:

$$Ra_L = \frac{g\beta(T_s - T_\infty)L^3}{\nu\alpha} \tag{5}$$

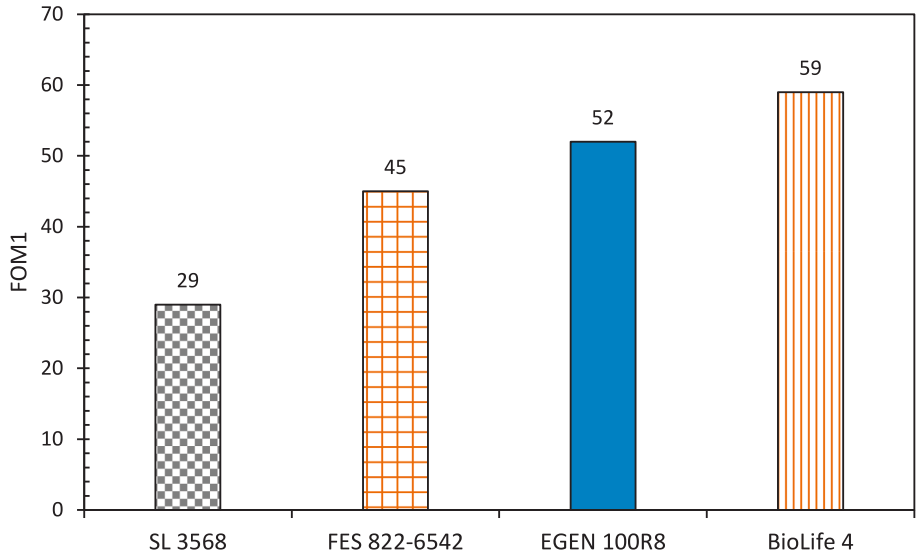

Fig. 3. FOM1 values for the four tested fluids.

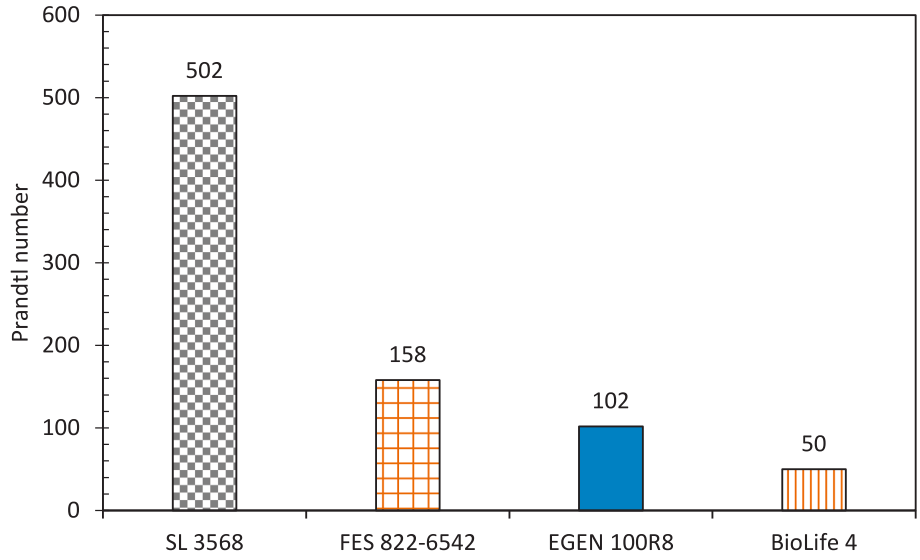

Fig. 4. Prandtl numbers for the four tested fluids.

Where T_s is the average server temperature (°C), T_∞ is the average fluid temperature (°C), L is the characteristic length of tank (m), g is the acceleration of gravity (m.s^{-2}), β is the thermal expansion coefficient of the fluid (K^{-1}), α is the thermal diffusivity of the fluid (m^2.s^{-1}) and ν is the kinematic viscosity of the fluid (m^2.s^{-1}).

Rayleigh numbers are calculated for each of the selected fluids to verify the relevance of the FOM1. Average server and fluid temperatures are listed in Table 3. Representative values are taken for an inlet temperature of 30 °C and a flow rate of 0.55 l.min^{-1}. The average server temperature, T_s, was calculated by considering the main heat-generating components directly in contact with the dielectric fluid, namely twelve RAM modules, six NVMEs, and two SSDs. It was computed as follows:

$$T_s = 0.6T_{RAM} + 0.3T_{NVME} + 0.1T_{SSD} \quad (6)$$

where T_{RAM} is the average RAM temperature, T_{NVME} is the average NVME temperature and T_{SSD} is the average SSD temperature.

Fig. 5 illustrates the Rayleigh number for each IC fluid. The Rayleigh numbers obtained for the tested fluids are consistent with the corresponding FOM1 trends. Hence FOM1 can be considered as a reliable indicator of the thermal performance of immersion fluids that cool IT components by natural convection. These conclusions must be confirmed by analyzing the experimental temperature values of the fluids and IT equipment.

Table 3
Average server and fluid temperatures for 30 °C water inlet temperature and a 0.55 l.min^{-1} flow rate.

Dielectric Fluid	Average server temperature T_s (°C)	Average fluid temperature T_∞ (°C)
SL 3568 (FOM1 = 29)	64	61.5
FES 822–6542 (FOM1 = 45)	59.7	56.3
EGEN 100R8 (FOM1 = 52)	57.1	54.3
BioLife 4 (FOM1 = 59)	56.9	54.1

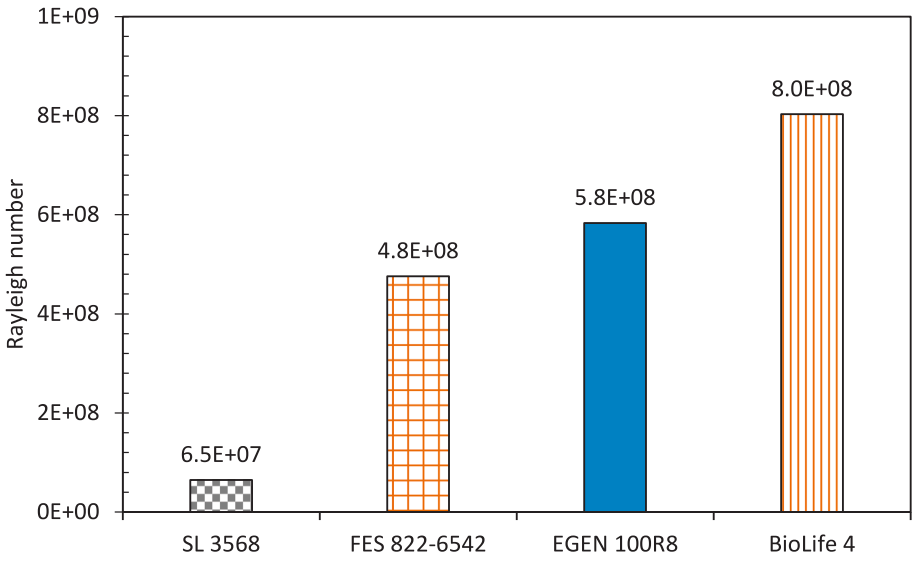

Fig. 5. Rayleigh number for the four tested fluids.

3.2.2. Effect of varying water flow rate and inlet water temperature on the fluid temperature

To assess the influence of various immersion coolants on the heat transfer capability of the hybrid SPIC system, the impact of different operating conditions on cooling performance were investigated.

3.2.2.1. Impact on the fluid temperature. Fig. 6 analyses further the effects of varying water flow rate and inlet water temperature on the average temperature of the four selected fluids. The fluids show globally similar thermal behavior, with comparable temperature trends observed for all tested conditions. The fluid temperature increases with rising inlet water temperature and decreases with increasing water flow rate. The average fluid temperature increases by approximately 7.6 %, respectively, when the water inlet temperature increases by 5 °C. Moreover, the fluid temperature decreases by approximately 2.9 % when the water flow rate increases by 0.05 $l.min^{-1}$. This reduction can be explained by the fact that a higher flow rate enhances the convective heat transfer between the serpentine coil and the dielectric fluid, thereby improving the overall thermal exchange efficiency. BioLife 4, with the highest FOM1, demonstrated the best thermal performance, exhibiting the lowest average temperature under all operating conditions. EGEN 100R8 was the second-best fluid and FES 822–6542 the third one based on the average temperature values. It should be noted that SL 3568 consistently resulted in the highest fluid temperatures. This classification confirms that immersion fluids with higher FOM1 values are more effective in maintaining lower average temperatures during server operation. It is noteworthy that, although BioLife4 has the lowest viscosity, it does not have the highest specific heat (FES 822–6542), thermal conductivity (EGEN 100R8), or thermal diffusivity (SL 3568). This finding highlights the importance of considering all fluid properties collectively when assessing thermal performance.

Fig. 7 illustrates the reduction in fluid temperature relative to SL 3568, which was chosen as the baseline due to its highest average temperature among the tested fluids. The maximum temperature

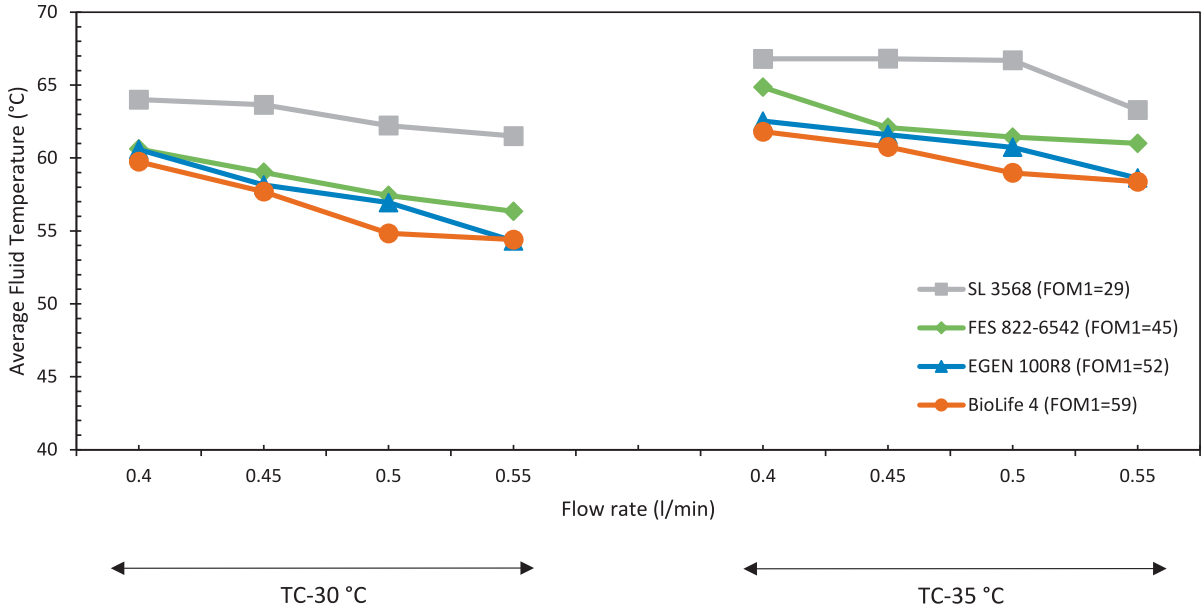

Fig. 6. Variations in the IC fluid temperature, under different temperatures conditions (TC) and flow rates, using SL 3568, FES 822–6542, EGEN 100R8, and BioLife 4 fluids.

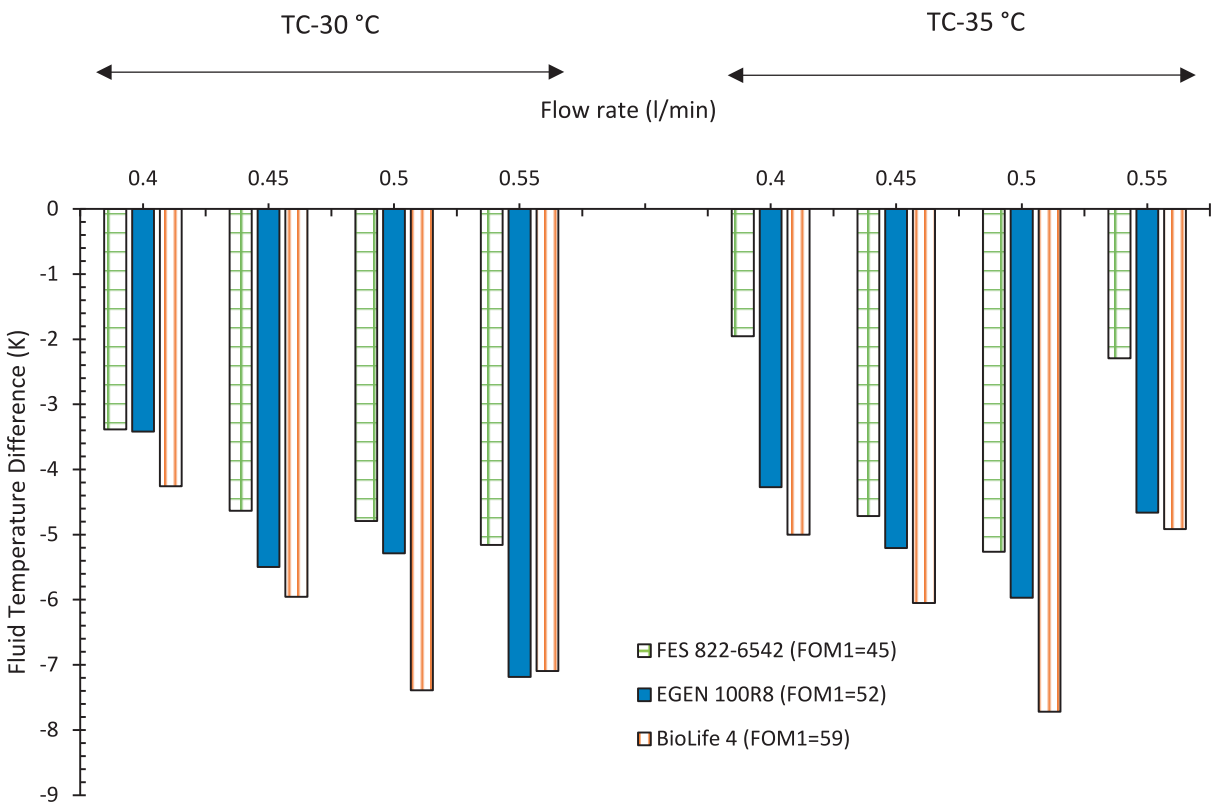

Fig. 7. Fluid temperature differences of FES 822–6542, EGEN 100R8 and BioLife 4 compared to SL 3568 as the baseline fluid.

reduction is observed at a flow rate of 0.5 l.min^{-1} for both inlet water temperature conditions. At this flow rate, the fluid temperatures decrease by approximately 7.9, 8.9 and 11.6 % when using FES 822–6542, EGEN 100R8 and BioLife 4 respectively. At the same flow rate, a temperature reduction of approximately 7.7 °C is achieved with BioLife 4, which corresponds to an approximative doubling of the FOM1 value compared to the baseline. These results further support the correlation between higher FOM1 values and improved fluid thermal performance in the hybrid SPIC system.

3.2.2.2. Impact on the IT temperatures. Fig. 8 a), b) and c) present the temperature variations of RAMs, NVMEs and SSDs components under different temperature and flow rate conditions, when using SL 3568, FES 822–6542, EGEN 100R8 and BioLife 4. These components exhibit broadly the same thermal behavior in each case. Statistical analysis indicates that their temperatures increase by approximately 6, 7.2 and 8 %, respectively, when the water inlet temperature increases by 5 °C. Moreover, their temperatures decrease by approximately 1.2, 5.9 and 5.6 %, respectively, when the water flow rate increases by 0.05 l.min^{-1}. As shown in Figure, RAM temperatures consistently remain below the critical limit of 78 °C regardless of operating conditions. Furthermore, RAMs, NVMEs and SSDs temperatures decrease by approximately 6.7, 6.4 and 5.9 °C respectively, when comparing BioLife 4 to SL 3568, which corresponds to an approximative doubling of the FOM1 value. These results align with the previously observed fluid temperature trends and can be attributed to the direct contact of these components with the immersion fluid.

Fig. 9 a) and b) present the temperature variations of the two CPUs (CPU0 and CPU1) under the different operating conditions. The water-cooling circuit is configured such that the flow is directed first through CPU0 and subsequently through CPU1. CPU0 and CPU1 exhibit broadly similar thermal behavior, with comparable temperature profiles observed for all four immersion fluids. As illustrated in Fig. 9 a) and b), CPU temperatures consistently remain below the critical limit of 95 °C, regardless of the inlet temperature and flow rate conditions. CPU0 and CPU1 temperatures increase by approximately 4.1 and 5.3 %, respectively, when the water inlet temperature increases by 5 °C. Moreover, their temperatures decrease by approximately 3.2 and 2.9 %, when the water flow rate increases by 0.05 l.min^{-1}.

In contrast to the other components (RAMs, NVMEs and SSDs), the CPUs exhibit an inverse thermal trend with respect to the FOM1 values of the dielectric fluids. Notably, the use of BioLife 4, which is the least viscous fluid, results in the highest CPU temperatures. This inversion is also confirmed for the other fluids.

It should be noted that, unlike the other IT components, the CPUs are not directly immersed in the dielectric fluid but are instead cooled via WBs. A thermal interface material (TIM), specifically the Kerafol Keratherm KP98 thermal paste, is applied between the CPU and the WB to enhance heat transfer. This TIM behaves as a highly viscous liquid, with a dynamic viscosity of 130 Pa.s, i.e. 5.9.10^4 cSt. The physical properties of the thermal paste are listed in Table 4. Moreover, a gasket is employed to prevent fluid penetration into the TIM, as illustrated in Fig. 10.

If the thermal paste is not adequately insulated from the dielectric fluid, there is a potential risk of the coolant penetrating the paste, leading to its partial degradation [39]. In such cases, direct contact between the immersion fluid and the TIM may result in mixing, thereby altering the physico-chemical properties of the paste and reducing its thermal performance. Specifically, the TIM may become less viscous, adversely affecting its heat transfer capability.

To evaluate the potential impact of the dielectric fluid on the degradation of the thermal paste, the viscosity of the resulting mixture—comprising KP98 paste and the immersion fluid—is estimated using Arrhenius' mixing law [40]. The viscosity of the mixture can be expressed as:

$$\ln(n) = x_1 \ln(n_1) + x_2 \ln(n_2) \tag{7}$$

where: n is the viscosity of the mixture (cSt), n_1 the viscosity of the thermal paste (cSt), n_2 the viscosity of the fluid (cSt), x_1 the mole frac-

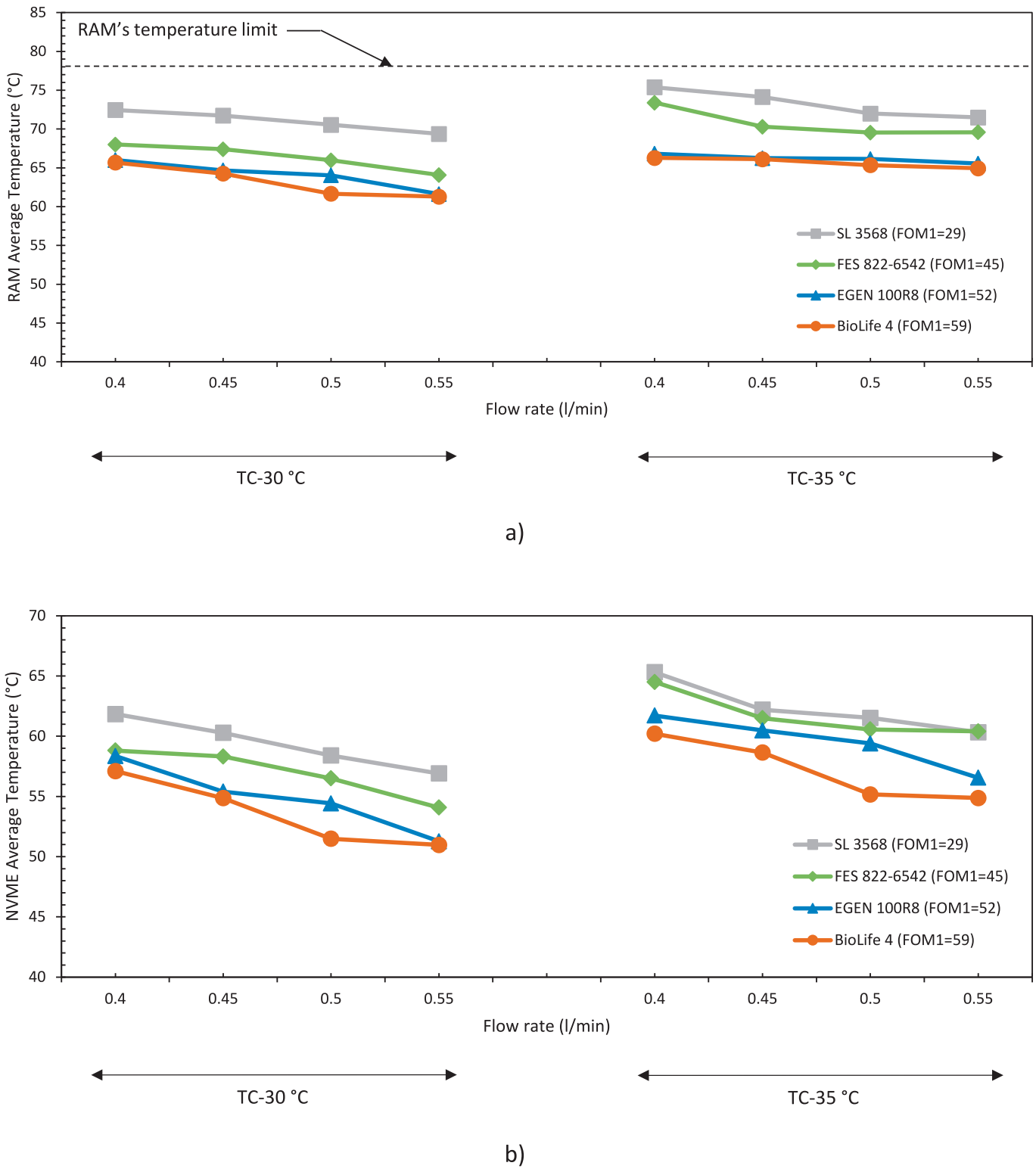

Fig. 8. Variations in (a) the RAMs, (b) NVMEs and (c) SSDs temperatures, under different temperature conditions and flow rates, using SL 3568, FES 822–6542, EGEN 100R8, and BioLife 4 fluids.

tion of the thermal paste and x_2 the mole fraction of the fluid.

The mole fractions are varied between 0.4 and 0.6 to realistically represent practical dilution scenarios.

Fig. 11 further analyses the effect of infiltration of immersion coolants on the viscosity of the KP98 and immersion fluid mixture. It is interesting to note a strong positive correlation is observed between the viscosity of the resulting mixture and that of the immersion fluid. Specifically, immersion fluids with lower viscosities tend to produce mixtures with significantly reduced viscosities, thereby indicating a higher degree of thermal paste degradation. The viscosity of the mixture is

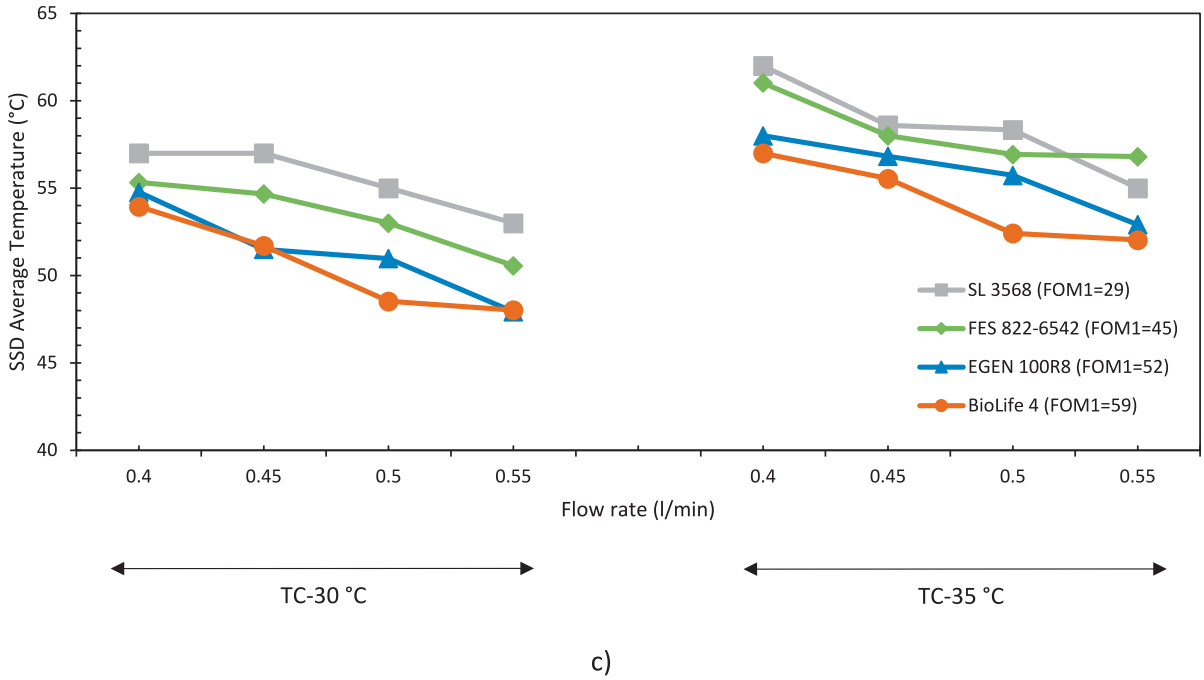

c)

Fig. 8. (*continued*).

reduced by at least 94.4 % compared to the initial viscosity of the TIM. This substantial reduction may account for the elevated CPU temperatures observed when using low-viscosity coolants. These findings suggest the necessity of either improving the insulation of the thermal paste from direct contact with the immersion fluid or selecting appropriate TIMs for immersion investigation.

4. Numerical methodology

To further evaluate the immersion fluids performance, this work investigated a heat transfer CFD analysis of a dielectric fluid and the immersed server experimentally tested.

4.1. Model description

In this study, SL 3568 fluid was selected for a model validation on a developed CAD model of the 620 W server. Other fluids will be investigated numerically in further work. The simulation was performed at a water inlet temperature of 30 °C and a water flow rate of 0.55 l.min^{-1} for the water-cooling circuit. The geometry is shown in Fig. 12.

The numerical simulation was carried out to understand the flow behavior of the dielectric coolant within the IC tank. The Ansys Fluent software was used for simulation, with turbulent flow conditions. The no-slip boundary conditions prevailed on the solid surfaces. The steady state, three dimensional, and incompressible flow assumptions were also considered. Thermal power densities were specified for the IT components and the tank walls are considered adiabatic. The volumetric heat losses were uniformly distributed throughout each IT component, a reasonable assumption when considering the heat-generating regions. Moreover, some fluid properties were given as a function of temperature as listed in Table 5, and the gravity effects were also included in the simulation. The electrical cables connected to the various server components were modeled as an equivalent porous medium. For the water-cooling circuit, a Velocity Inlet boundary condition was imposed at the inlet, while an Outflow boundary condition was applied at the outlet. In addition, the computation time ranged from 40 s to 1 min per iteration.

The continuity, momentum, and energy equations are simultaneously solved to predict the flow field and temperature distribution in the IC tank. The continuity, momentum, and energy equations are listed below,

Continuity equation:

$$\nabla\cdot\vec{V}=0 \tag{8}$$

Momentum equation:

$$\rho\left(\vec{V}.\nabla\right)\vec{V}=-\nabla P+\nabla\cdot\mu\nabla\vec{V}+\nabla\cdot\tau_{turbulent}+\rho\vec{g} \tag{9}$$

Energy equation:

$$(\rho C_p)\vec{V}.\nabla T=\nabla\cdot k\nabla T \tag{10}$$

where ρ is the density of the dielectric fluid (kg.m^{-3}), P is the pressure (Pa), μ is the dynamic viscosity (Pa.s), T is the temperature (°C), k is the thermal conductivity (W.m^{-1} K^{-1}), $\vec{g}$ is the acceleration due to gravity (m.s^{-2}), and $\vec{V}$ is the velocity vector (m.s^{-1}).

The term $\tau_{turbulent}$ represents the Reynolds stress tensor based on an eddy viscosity assumption. The standard k–ε turbulence model was employed in combination with the Enhanced Wall Treatment approach to accurately capture the effects of the viscous sublayer and resolve temperature gradients near hot surfaces, thus ensuring a reliable description of natural convection effects [41]. To ensure numerical stability and improve convergence behavior, a pseudo-transient solution method was adopted together with a Coupled pressure–velocity scheme. Spatial discretization was performed using the Second-Order Upwind scheme for all transport equations, except for the pressure equation, for which the Body Force Weighted scheme was applied due to the dominant influence of body forces on the flow field.

4.2. Grid independence analysis

The temperature of the two CPUs and the fluid at seven locations were considered as parameters to verify the mesh sensitivity on the numeric results. Meshes of approximately 8, 15, 31, and 85 million cells were compared. The mesh consists of hexahedral cells (boundary layers) and polyhedral cells. Besides, the mesh was locally refined near the CPUs. As reported in Table 6 and Table 7, the CPUs and fluid

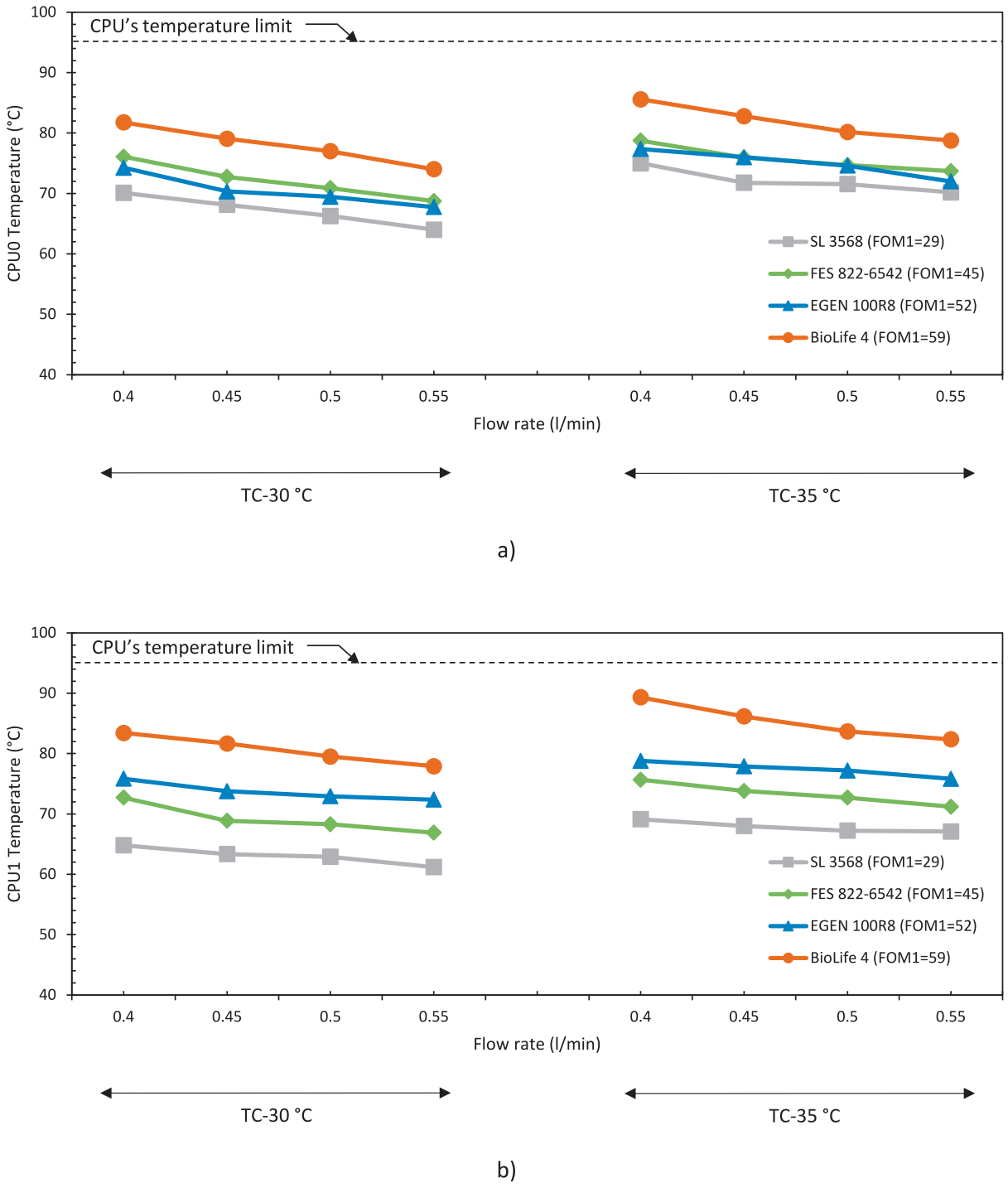

Fig. 9. Variations in (a) CPU0 and (b) CPU1 temperatures, under different temperature conditions and flow rates, using SL 3568, FES 822–6542, EGEN 100R8, and BioLife 4 fluids.

Table 4
KP98 TIM physical properties.

Property	Specification
Thermal conductivity ($W.m^{-1}K^{-1}$)	6
Density (g/cm^3)	2.2
Viscosity ($.10^4$ cSt)	5.9

temperatures showed variations of about 0.5 % and less than 1.5 % respectively, when the number of mesh elements was increased to nearly 15 million, which was not the case for the 8-million-cell mesh. Hence, the model with 15 million cells, with a minimum cell size of 0.25 mm, was adopted for further numerical simulation as it offered a suitable compromise between accuracy and computational cost. In particular, the 31 million-cell mesh required approximately 1.67 times more computational time than the 15 million-cell mesh, without providing significant improvements in accuracy.

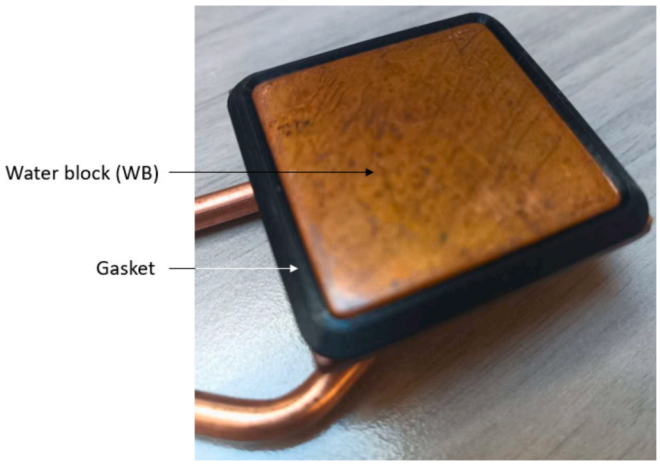

Fig. 10. Photo of the seal gasket fixed around the water block base copper surface.

4.3. Results and discussion

For the analysis, fluid temperature fields and component temperatures were modelled and the CFD model is validated by comparing with the experimental results.

4.3.1. Water and fluid behavior

Fig. 13 illustrates the temperature distribution of CPU0 in a horizontal plane intersecting its midsection. It is shown that CPU0 is cooled by the WB, independently of the dielectric fluid. The thermal energy generated by CPU0 is transferred to the water-cooling system through the CPU casing. In addition, the temperature field reveals an apparent gradient, with higher temperatures observed on the motherboard support side compared to the water-cooling side. This temperature distribution effectively characterizes the conductive heat diffusion near the CPUs. Since the temperature sensors measuring the CPUs' temperature are located close to the motherboard support side, the reported CPU temperature values are in good agreement with the experimental measurements. Moreover, it is noteworthy that the surface temperature of the water block is weakly impacted by the surrounding hot dielectric fluid, while a local temperature gradient is still observed in the fluid region around the water block.

The variation of the fluid temperature represented with 3D current lines is presented in Fig. 14. Streamlines are plotted from the interfaces of the power supply. The figure reveals a thermal gradient with maximum temperatures occurring in the upper region and minimum values near the bottom. At the right region, a notable increase in temperature is observed in the vertical direction, particularly across the power supply. In contrast, a descending flow pattern is observed along the serpentine coil at the left-hand side, where the dielectric fluid is cooled. Therefore, these streamlines confirm that the convective motion within the system is governed by natural convection. The numerical calculation indicated an average dielectric fluid temperature of 62 °C, compared to the experimental value of 61.5 °C, representing a negligible variation of 0.8 %.

4.3.2. IT components behavior

Fig. 15 shows the surface temperature of the IT components. The temperature field shows ascending thermal plumes characteristic of natural convection. The CPU0, CPU1, RAMs and NVMEs reached temperatures of 59.3, 64.9, 73 and 50 °C, respectively. The RAM modules exhibit similar thermal behavior since they are positioned along the same horizontal alignment. In contrast, the power supply unit displays a non-uniform surface temperature distribution, which can be attributed to the vertical thermal stratification of the dielectric fluid inside the tank. A comparison of experimental data and numerical results for the RAMs, NVMEs, CPU0 and CPU1 is plotted in Table 8. As indicated, the average temperature of the RAMs, NVMEs, CPU0 and CPU1 simulated numerically fits well with the measurement data from the experiments with a maximum difference of 10.7 % for NVMEs. This deviation could be attributable to the thermal dissipation of the NVMEs. Indeed, the model assumes a volumetric thermal dissipation across all the NVMEs. Under practical conditions, the heat generation within the NVMEs is more localized, which affects the measured temperature of the components, especially if the temperature sensor is located close to the NVME's heat source. These results support the reliability of the current simulation method for evaluating the thermal performance of different candidate fluids for immersion cooling.

5. Conclusion

This paper investigates the cooling performance of different immersion fluids in a hybrid single-phase liquid-cooling system, where CPUs are cooled by direct-to-chip cold plates and other server

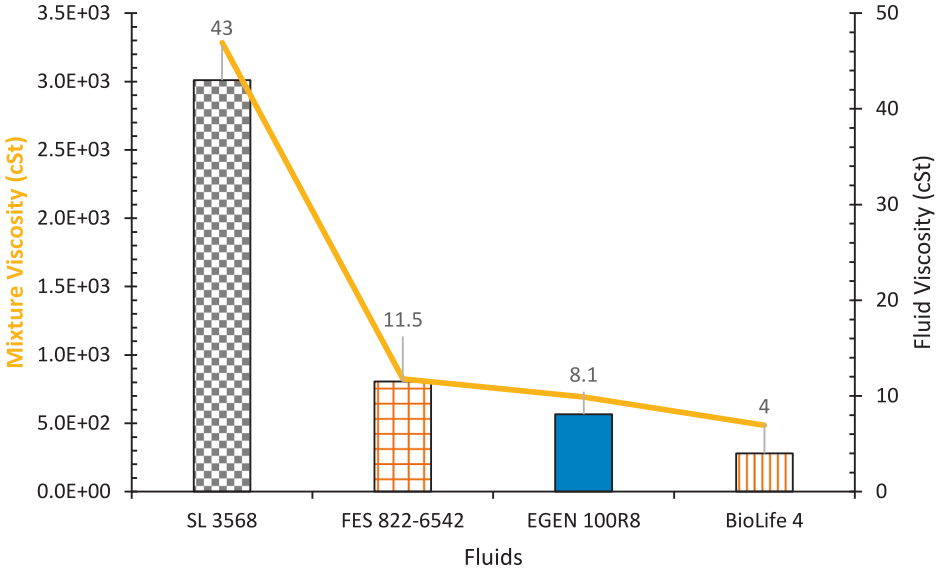

Fig. 11. Evolution of the viscosity of the mixture (KP98 & immersion fluid) for the four tested fluids.

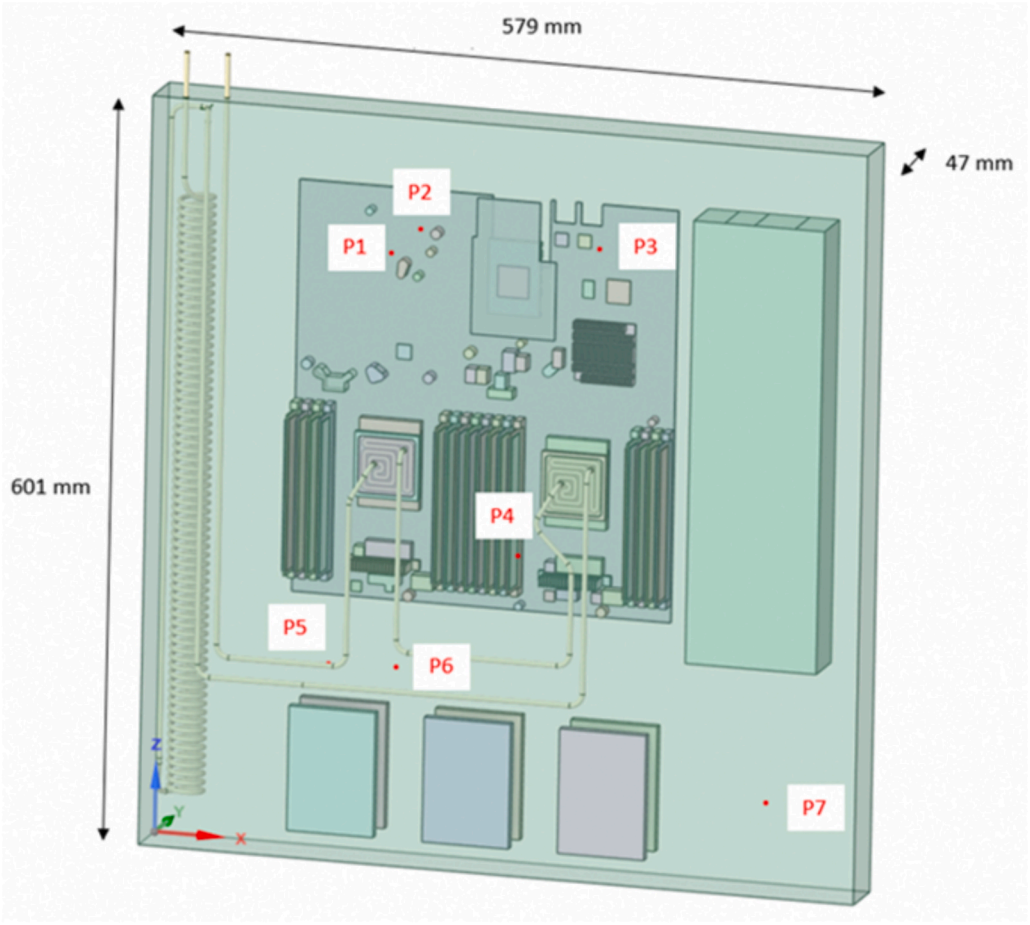

Fig. 12. Scheme of the 3D model geometry with fluid temperature measurement locations.

Table 5
Thermophysical properties of SL 3568 fluid at different temperatures.

Properties at	0 °C	40 °C	100 °C
Density (kg.m^{-3})	838	812	773
Kinematic viscosity (cSt)	406	43	7.6
Thermal conductivity (W.m^{-1}.K^{-1})	0.142	0.139	0.134
Specific heat (kJ.kg^{-1}K^{-1})	1.85	2	2.23

Table 6
Average CPU0, CPU1 and local fluid temperatures in °C for 8, 15, 31 and 85 million cell meshes.

	8-million-cell mesh	15-million-cell mesh	31-million-cell mesh	85-million-cell-mesh
CPU0	59.4	59.3	59.2	59.0
CPU1	65.1	64.9	64.7	64.6
P1	77.5	77.9	77.7	78.0
P2	80.2	80.7	80.6	81.2
P3	79.8	80.3	80.4	81.0
P4	62.1	61.5	61.1	61.1
P5	45.2	45.2	44.9	44.6
P6	44.4	44.5	44.2	44.0
P7	43.9	43.9	43.8	43.8

components (Motherboard, RAMs, NVMEs, SSDs…) are cooled by immersion. An experimental setup was used to assess four dielectric fluids — SL 3568, FES 822–6542, EGEN 100R8, and BioLife 4 — with thermal performance evaluated using the Figure of Merit FOM1 indicator for buoyancy-driven systems, as defined by the OCP Immersion Cooling Sub-Project. The selection of these dielectric fluids offers insights into

Table 7
Relative errors in % on average CPU0, CPU1 and local fluid temperatures with respect to the 85-million-cell mesh.

	8-million-cell mesh	15-million-cell mesh	31-million-cell mesh	85-million-cell-mesh
CPU0	0.70	0.53	0.35	Reference
CPU1	0.80	0.48	0.16	Reference
P1	−0.63	−0.16	−0.47	Reference
P2	−1.21	−0.61	−0.76	Reference
P3	−1.52	−0.91	−0.76	Reference
P4	1.63	0.61	0.00	Reference
P5	1.36	1.36	0.62	Reference
P6	0.99	1.23	0.49	Reference
P7	0.26	0.26	0.00	Reference

different development focuses such as diverse viscosity grades, flash point and biodegradability. A CFD model is validated against experimental results to enable a broader evaluation and selection of candidate immersion coolants. According to the above investigations, the following conclusions could be drawn.

- When FOM1 is approximately doubled (BioLife 4 compared to SL 3568), a Prandtl number roughly ten times smaller could be obtained, that indicates that the influence of the convective flow on heat diffusion in the coolant is nearly reduced by a factor of ten.
- The fluids exhibiting the highest FOM1 demonstrated the lowest average temperatures. Specifically, a near doubling of FOM1 resulted in a decrease in fluid temperature by approximately 7.7 °C.

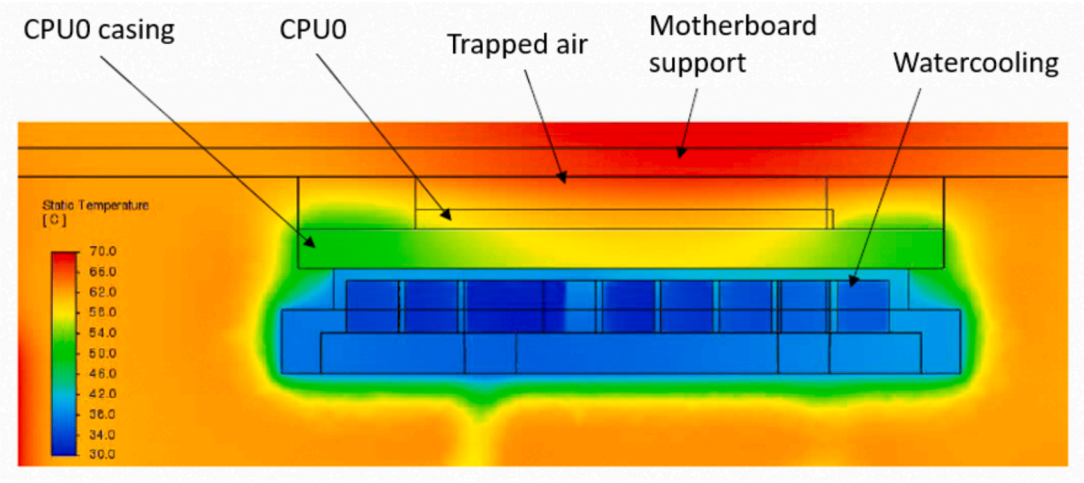

Fig. 13. Temperature distribution of CPU0 in a horizontal plane intersecting its midsection.

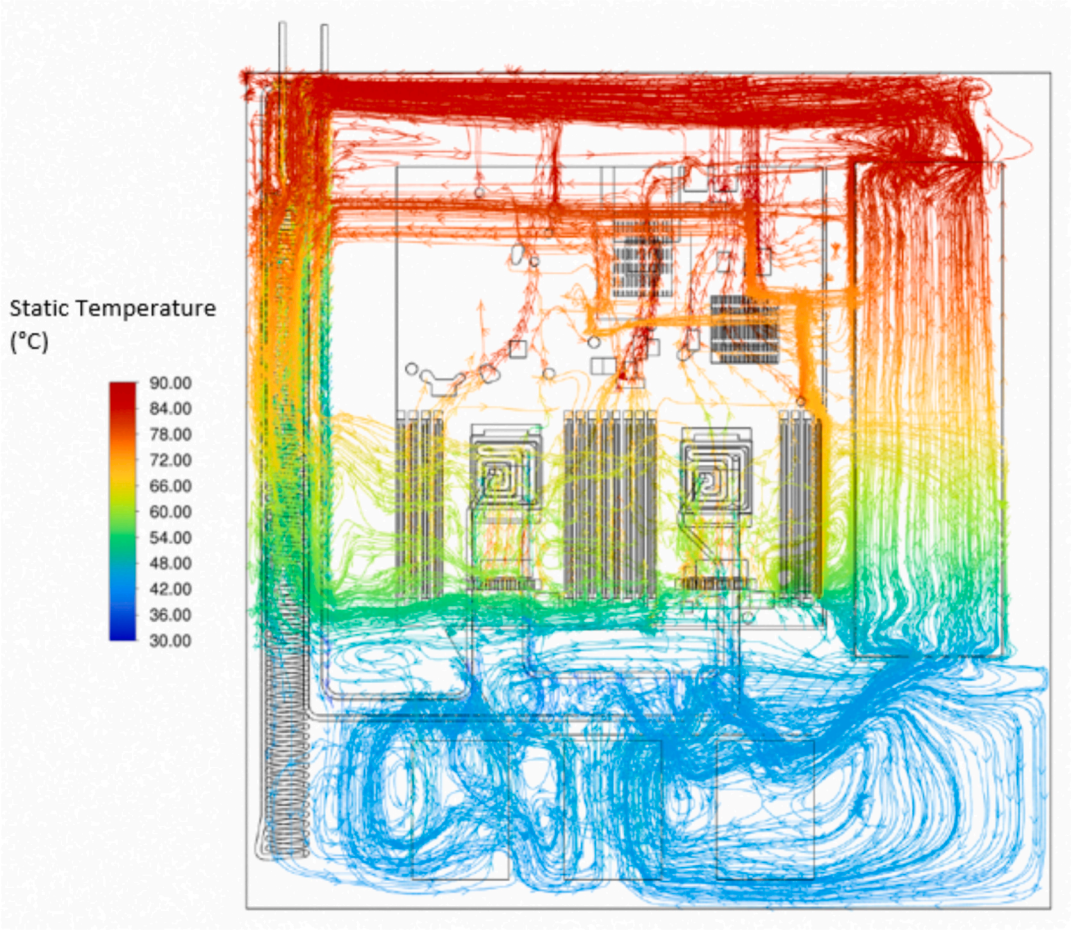

Fig. 14. 3D temperature streamlines of SL 3568 fluid.

- As expected, RAMs, NVMEs and SSDs, which are in direct contact with the dielectric fluids, exhibited the lowest temperatures when using high-FOM1 coolants. Their temperatures decreased by approximately 6.7, 6.4 and 5.9 °C respectively, when FOM1 was roughly doubled.
- The highest CPU temperatures were observed when using the fluids with the greatest FOM1 values. It is demonstrated that this inverse trend is probably due to partial infiltration of the dielectric fluid into the thermal paste (TIM) applied between the CPUs and the WBs.
- The numerical results fit well with the experimental ones with a maximum temperature deviation of 10.7 %, for NVMEs average temperature. Thereby the CFD model could be used to compare a variety of immersion coolants proposed in the industry.

Finally, the fluids with the highest FOM1 values appear to be the

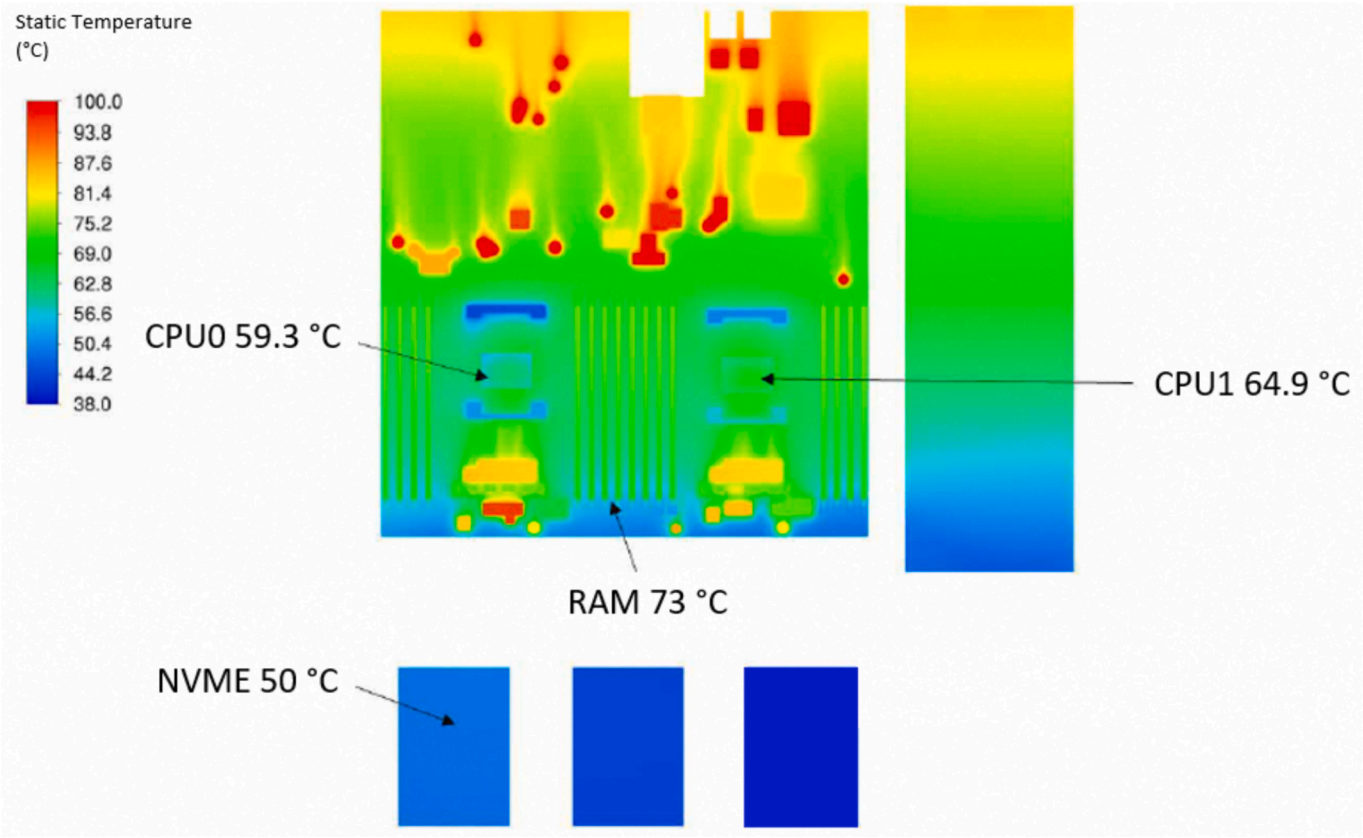

Fig. 15. Surface temperature of the IT components.

Table 8
IT behavior temperature comparison between experimental and CFD model.

IT components	Numerical average temperature (°C)	Experimental average temperature (°C)	Error (%)
RAM	73	69.4	5.2
NVME	50	56	−10.7
CPU0	59.3	61.2	−3.4
CPU1	64.9	64	1.4

most effective for components cooled directly by immersion. However, we observed potential incompatibility issues with the thermal interface material (TIM) when using very low-viscosity fluids (i.e., those with higher FOM1 values). Future work should therefore further investigate equipment compatibility, particularly the TIM, with such fluids. In addition, evaluating FOM1 locally in different regions of the dielectric fluid would help account for temperature-dependent properties. This would also provide a better assessment of flow resistance within the tank and reveal whether significant variations occur.

CRediT authorship contribution statement

Ayoub Ruichek: Writing – original draft, Software, Investigation, Formal analysis, Data curation, Conceptualization. **Mohamad Hnayno:** Writing – review & editing, Validation, Software, Methodology, Formal analysis, Conceptualization. **Ali Chehade:** Project administration, Methodology, Funding acquisition. **Farouk Fardoun:** Writing – review & editing. **Tala Moussa:** Writing – review & editing, Validation, Formal analysis. **Guillaume Polidori:** Writing – review & editing. **Chadi Maalouf:** Validation, Supervision, Methodology, Funding acquisition.

Declaration of competing interest

The authors declare that they have no known competing financial interests or personal relationships that could have appeared to influence the work reported in this paper.

Acknowledgement

The authors wish to thank the French National Agency for Technological Research (ANRT) for their funding and the dielectric fluid suppliers: Shell for SL 3568, Fuchs for FES 822-6542, Motul for EGEN 100R8, and TotalEnergies Fluids for BioLife 4. We also thank the R&D team from OVHcloud for their help during the experimental tests.

Data availability

Data will be made available on request.

References

[1] D. Mytton, M. Ashtine, Sources of data center energy estimates: a comprehensive review, Joule 6 (2022) 2032–2056, https://doi.org/10.1016/j.joule.2022.07.011.
[2] A. Khosravi, O.R. Sandoval, M.S. Taslimi, T. Sahrakorpi, G. Amorim, J.J. Garcia Pabon, Review of energy efficiency and technological advancements in data center power systems, Energy and Buildings 323 (2024) 114834, https://doi.org/10.1016/j.enbuild.2024.114834.
[3] M. Koot, F. Wijnhoven, Usage impact on data center electricity needs: a system dynamic forecasting model, Appl. Energy 291 (2021) 116798, https://doi.org/10.1016/j.apenergy.2021.116798.
[4] M.K. Patterson, in: The Effect of Data Center Temperature on Energy Efficiency, in, 2008, pp. 1167–1174, https://doi.org/10.1109/ITHERM.2008.4544393.
[5] A.A. Alkrush, M.S. Salem, O. Abdelrehim, A.A. Hegazi, Data centers cooling: a critical review of techniques, challenges, and energy saving solutions, Int. J. Refrig 160 (2024) 246–262, https://doi.org/10.1016/j.ijrefrig.2024.02.007.
[6] Q. Zhang, Z. Meng, X. Hong, Y. Zhan, J. Liu, J. Dong, T. Bai, J. Niu, M.J. Deen, A survey on data center cooling systems: Technology, power consumption

modeling and control strategy optimization, J. Syst. Archit. 119 (2021) 102253, https://doi.org/10.1016/j.sysarc.2021.102253.
[7] C. Nadjahi, H. Louahlia, S. Lemasson, A review of thermal management and innovative cooling strategies for data center, Sustainable Computing: Informatics and Systems 19 (2018) 14–28, https://doi.org/10.1016/j.suscom.2018.05.002.
[8] W.-X. Chu, C.-C. Wang, A review on airflow management in data centers, Appl. Energy 240 (2019) 84–119, https://doi.org/10.1016/j.apenergy.2019.02.041.
[9] M. Saini, R.L. Webb, Heat rejection limits of air cooled plane fin heat sinks for computer cooling, in: ITherm 2002. Eighth Intersociety Conference on Thermal and Thermomechanical Phenomena in Electronic Systems (Cat. No.02CH37258), 2002: pp. 1–8. Doi: 10.1109/ITHERM.2002.1012431.
[10] A detailed Study on Data Centre Energy Efficiency and Efficient Cooling Techniques, IJATCSE 9 (2020) 9221–9242. Doi: 10.30534/ijatcse/2020/332952020.
[11] Y. Blosch, Air Cooling vs. Liquid Immersion Cooling: Can Liquid Immersion Cooling Improve the Energy and Space Efficiency of Data Centres?, (n.d.).
[12] A. Habibi Khalaj, S.K. Halgamuge, A,, Review on efficient thermal management of air- and liquid-cooled data centers: from chip to the cooling system, Applied Energy (2017) 1165–1188.
[13] M. Azarifar, M. Arik, J.-Y. Chang, Liquid cooling of data centers: a necessity facing challenges, Appl. Therm. Eng. 247 (2024) 123112, https://doi.org/10.1016/j.applthermaleng.2024.123112.
[14] R. Kong, H. Zhang, M. Tang, H. Zou, C. Tian, T. Ding, Enhancing data center cooling efficiency and ability: a comprehensive review of direct liquid cooling technologies, Energy 308 (2024) 132846, https://doi.org/10.1016/j.energy.2024.132846.
[15] Y. Zhang, C. Li, M. Pan, Design and performance research of integrated indirect liquid cooling system for rack server, Int. J. Therm. Sci. 184 (2023) 107951, https://doi.org/10.1016/j.ijthermalsci.2022.107951.
[16] P. Shahi, A. Heydari, C. Hinge, L.S.R. Chinthaparthy, H. Modi, H. Miyamura, M. Tradat, U. Chowdhury, V. Radmard, D. Agonafer, J. Rodriguez, Thermal, Hydraulic and Reliability Analysis of Single-phase Liquid Coolants for Direct-to-Chip Cold Plate Cooling in High-Performance Computing Systems, American Society of Mechanical Engineers Digital Collection (2023), https://doi.org/10.1115/IPACK2023-110576.
[17] Enhancement of heat transfer in cooling channels for electronic devices using multi-directional graded triply periodic minimal surfaces (TPMS) | Request PDF, (n.d.). https://www.researchgate.net/publication/386308105_Enhancement_of_heat_transfer_in_cooling_channels_for_electronic_devices_using_multi-directional_graded_triply_periodic_minimal_surfaces_TPMS (accessed April 2, 2025).
[18] K. Haghshenas, B. Setz, Y. Blosch, M. Aiello, Enough hot air: the role of immersion cooling, Energy Inform 6 (2023) 14, https://doi.org/10.1186/s42162-023-00269-0.
[19] N.A. Pambudi, A. Sarifudin, R.A. Firdaus, D.K. Ulfa, I.M. Gandidi, R. Romadhon, The immersion cooling technology: current and future development in energy saving, Alex. Eng. J. 61 (2022) 9509–9527, https://doi.org/10.1016/j.aej.2022.02.059.
[20] C.-K. Liu, T.-Y. Chang, Thermal Performance of Single-Phase and Two-Phase Immersion Cooling in Data Center, in: 2022 17th International Microsystems, Packaging, Assembly and Circuits Technology Conference (IMPACT), 2022: pp. 1–4. Doi: 10.1109/IMPACT56280.2022.9966684.
[21] Chethana Gorur Dharanegowda, Bommegowda Sadashive Gowda, Investigation of Single-Phase Immersion Cooling for Modern Data Centers, ARFMTS 111 (2024) 141–153, https://doi.org/10.37934/arfmts.111.2.141153.
[22] A. Vagiakis, D.N. Korres, C. Tzivanidis, Simulation of natural convection heat transfer in dielectric liquids for single-phase immersion cooling rack server, Appl. Therm. Eng. 274 (2025) 126595, https://doi.org/10.1016/j.applthermaleng.2025.126595.
[23] Y. Huang, J. Ge, Y. Chen, C. Zhang, Natural and forced convection heat transfer characteristics of single-phase immersion cooling systems for data centers, Int. J. Heat Mass Transf. 207 (2023) 124023, https://doi.org/10.1016/j.ijheatmasstransfer.2023.124023.
[24] X. Sun, Z. Liu, S. Ji, K. Yuan, Experimental study on thermal performance of a single-phase immersion cooling unit for high-density computing power data center, Int. J. Heat Fluid Flow 112 (2025) 109735, https://doi.org/10.1016/j.ijheatfluidflow.2024.109735.
[25] Z. Liu, X. Sun, S. Ji, K. Yuan, A multi-objective optimization of a single-phase immersion cooling system at cabinet level, Energ. Buildings 312 (2024) 114221, https://doi.org/10.1016/j.enbuild.2024.114221.
[26] B.B. Kanbur, C. Wu, S. Fan, W. Tong, F. Duan, Two-phase liquid-immersion data center cooling system: Experimental performance and thermoeconomic analysis, Int. J. Refrig 118 (2020) 290–301, https://doi.org/10.1016/j.ijrefrig.2020.05.026.
[27] H. Wang, X. Yuan, K. Zhang, X. Lang, H. Chen, H. Yu, S. Li, Performance evaluation and optimization of data center servers using single-phase immersion cooling, Int. J. Heat Mass Transf. 221 (2024) 125057, https://doi.org/10.1016/j.ijheatmasstransfer.2023.125057.
[28] N. Agung Pambudi, A. Muhamad Yusuf, A. Sarifudin, The use of Single-phase Immersion Cooling by using two Types of Dielectric Fluid for Data Center Energy Savings, Energy Engineering 119 (2022) 275–286, https://doi.org/10.32604/EE.2022.017356.
[29] Q. Luo, C. Wang, H. Wen, L. Liu, Research and optimization of thermophysical properties of sic oil-based nanofluids for data center immersion cooling, Int. Commun. Heat Mass Transfer 131 (2022) 105863, https://doi.org/10.1016/j.icheatmasstransfer.2021.105863.
[30] H. Shrigondekar, Y.-C. Lin, C.-C. Wang, Investigations on performance of single-phase immersion cooling system, Int. J. Heat Mass Transf. 206 (2023) 123961, https://doi.org/10.1016/j.ijheatmasstransfer.2023.123961.
[31] X. Chen, Y. Huang, S. Xu, C. Bao, Y. Zhong, Y. Chen, C. Zhang, Thermal performance evaluation of electronic fluorinated liquids for single-phase immersion liquid cooling, Int. J. Heat Mass Transf. 220 (2024) 124951, https://doi.org/10.1016/j.ijheatmasstransfer.2023.124951.
[32] J. Kim, H. Choi, S. Lee, H. Lee, Computational study of single-phase immersion cooling for high-energy density server rack for data centers, Appl. Therm. Eng. 264 (2025) 125476, https://doi.org/10.1016/j.applthermaleng.2025.125476.
[33] F.S. Alkasmoul, A.M. Almogbel, M.W. Shahzad, A.J. Al-damook, Thermal performance and optimum concentration of different nanofluids in immersion cooling in data center servers, Results Eng. 25 (2025) 103699, https://doi.org/10.1016/j.rineng.2024.103699.
[34] R. Brink, Base Specification for Immersion Fluids, (n.d.).
[35] T.H. Kim, D.-K. Kim, K.H. Do, Correlation for the fin Nusselt number of natural convective heat sinks with vertically oriented plate-fins, Heat Mass Transfer 49 (2013) 413–425, https://doi.org/10.1007/s00231-012-1100-0.
[36] M. Hnayno, A. Chehade, H. Klaba, G. Polidori, C. Maalouf, Experimental investigation of a data-centre cooling system using a new single-phase immersion/liquid technique, Case Stud. Therm. Eng. 45 (2023) 102925, https://doi.org/10.1016/j.csite.2023.102925.
[37] R.J. Moffat, Describing the uncertainties in experimental results, Exp. Therm Fluid Sci. 1 (1988) 3–17, https://doi.org/10.1016/0894-1777(88)90043-X.
[38] C. Varga, S. Fohanno, G. Polidori, Turbulent boundary-layer buoyant flow modeling over a wide Prandtl number range, Acta Mech. 172 (2004) 65–73, https://doi.org/10.1007/s00707-004-0135-9.
[39] L. Yu, J. Yang, D. Shia, M. Zhang, A study on compatibility of thermal interface materials with coolants for data center immersion cooling, in: In: 2022 21st IEEE Intersociety Conference on Thermal and Thermomechanical Phenomena in Electronic Systems (iTherm), 2022, pp. 1–5, https://doi.org/10.1109/iTherm54085.2022.9899572.
[40] S. Arrhenius, The Viscosity of Solutions, Biochem. J 11 (1917) 112–133.
[41] 4.18.2. Wall Treatment for ε-based Models, (n.d.). https://ansyshelp.ansys.com/public/account/secured?returnurl=////Views/Secured/corp/v242/en/flu_th/ch04s18s02.html (accessed August 18, 2025).